CCVD Synthesis of Carbon-Encapsulated Cobalt Nanoparticles for Biomedical Applications

Petar Lukanov, Vijay K. Anuganti, Yulia Krupskaya, Anne-Marie Galibert, Brigitte Soula, Carmen Tîlmaciu, Aldrik H. Velders, Ruediger Klingeler, Bernd Büchner, Emmanuel Flahaut

CCVD Synthesis of Carbon-Encapsulated Cobalt Nanoparticles for Biomedical Applications

*Petar Lukanov, Vijay K. Anuganti, Yulia Krupskaya, Anne-Marie Galibert, Brigitte Soula, Carmen Tilmaciu, Aldrik H. Velders, Ruediger Klingeler, Bernd Büchner, and Emmanuel Flahaut**

Carbon-encapsulated ferromagnetic Cobalt nanoparticles (Co@C) have been synthesized by catalytic chemical vapour deposition (CCVD). The nanoparticles, mainly ranging between 10 and 15 nm, are tightly encapsulated by 2–3 concentric graphitic carbon shells and protected from oxidation. Because of their magnetic properties (saturation magnetization of 106 emu/g and a coercivity HC of 250 Oe), Co@C nanoparticles have been investigated for hyperthermia application. Although the observed values of the specific absorption rate (28.7 W/gCo@C at 30 kA/m and 215.4 W/gCo@C at 70 kA/m) are slightly lower than required in actual hyperthermia therapies, the observed strong heating effect provides a very promising starting point for future clinical application. It is also demonstrated that these nanoparticles can at the same time be used for magnetic resonance imaging (MRI) with an efficiency comparable to commercially available T2 contrast agents.

1. Introduction

In the last decades encapsulated magnetic particles have been proposed and are now already used for various applications including electrochemical energy storage[1] or magnetic resonance imaging.[2,3] Carbon-encapsulated metal nanoparticles have received considerable attention because of their high chemical and thermal stabilities.[4–6] This applies in particular for medical applications where the coating of the nanoparticles with different materials like carbon shells or surfactant brings many advantages.[7,8] Bystrejewski et al.[9] reported an arc-plasma method for carbon-encapsulation of magnetic FeNdB nanoparticles for potential bioapplication in drug delivery, cancer therapy or magnetic resonance imaging (MRI). Several preparation methods, such as thermal decomposition of organic complexes,[10] arc-discharge (or modified arc-discharge)[11] or CVD (chemical vapour deposition) have been employed. The arc-discharge method is the most popular but the CVD method should be considered for future industrial fabrication of carbon-encapsulated magnetic nanoparticles. Ruoff et al.[11] first used arc-discharge synthesis for the preparation of carbon-encapsulated single-crystal LaC_2 nanoparticles with sizes up to 40 nm. Following this procedure Saito et al.[12,13] managed to encapsulate magnetic materials like Co and Co_3C (50–200 nm), and most of the rare-earth metals (Sc, Y, La, Ce, Pr, Nd, Gd, Tb, Dy, Ho, Er, Lu, Sm, Eu and Yb). Due to the low costs, high yield and simplicity, the CCVD method is a good candidate for future industrial fabrication of carbon-encapsulated magnetic nanoparticles, such as Co.[14] Flahaut et al.[15] reported the CCVD preparation of very small carbon-encapsulated cobalt nanoparticles (5–15 nm) involving reduction by a H_2/CH_4 mixture of a $Mg_{1-X}Co_XO$ solid solution. In general, this method was used by the same authors to produce carbon nanotubes[16] but it was mentioned that when the CCVD conditions are correctly adapted, encapsulation of the catalytic nanoparticles by carbon shells with very limited CNT growth can be favoured. Recently, the CCVD method was successfully used in order to produce Fe/Co,[17] Ni[18] and Au[19] nanoparticles coated by carbon shells for magnetic resonance imaging or biofunctionalisation. CCVD was considered as the only viable method to synthesize carbon-encapsulated Fe nanoparticles.[20] Experimentally, Co@C nanoparticles were found to exhibit a higher saturation magnetization (M_s) than Fe@C or Ni@C.[21,22] Another advantage of forming Co@C is that the samples contain no other phase (e.g., carbides) while the encapsulation prevents the oxidation of the small metal nanoparticles.

Here we report the synthesis of Co@C nanoparticles with

Dr. P. Lukanov, Dr. A.-M. Galibert, Dr. B. Soula, C. Tilmaciu,
Dr. E. Flahaut
Université de Toulouse
UPS, INP, Institut Carnot Cirimat
118, route de Narbonne
F- 31062 Toulouse, France
CNRS, Institut Carnot Cirimat
F-31062 Toulouse, France
E-mail: flahaut@chimie.ups-tlse.fr
V. K. Anuganti, Dr. A. H. Velders
SupraMolecular Chemistry and Technology
MESA+ Institute for Nanotechnology
University of Twente
7500 AE Enschede, The Netherlands
Y. Krupskaya, Prof. B. Büchner
Leibniz Institute for Solid State and Materials Research - IFW Dresden
Helmholtzstraße 20, 01069 Dresden, Germany
Prof. R. Klingeler
Kirchhoff Institute for Physics
Heidelberg University
INF 227, 69120 Heidelberg, Germany

initially proposed by Flahaut et al.[15] who successfully synthesized very small Co@C nanoparticles, we modified the CCVD conditions in order to improve and adapt the properties of the final product to the requirements of biomedical applications such as diagnostics, i.e,. magnetic resonance imaging (MRI) contrast agents or therapeutics such as hyperthermia for localized cancer treatment. In our work, Co nanoparticles were formed by selective reduction of a $Mg_{0.92}Co_{0.08}O$ solid solution by a H_2–CH_4 gas mixture leading to their fast and tight encapsulation by graphitic carbon shells. Moreover, we investigated the magnetic properties of the synthesized Co@C nanoparticles and tested their applicability for both magnetic hyperthermia and as MRI contrast agent.

Magnetic resonance imaging (MRI) is a powerful non-invasive diagnostic technique used in clinical medicine for in vivo assessment of anatomy and biological function. The current MRI contrast agents in clinical use are in the form of either paramagnetic complexes[23] or superparamagnetic iron oxide nanoparticles (SPIO).[7,24] Paramagnetic complexes, which are usually gadolinium (Gd^{3+}) or manganese (Mn^{2+}) chelates, accelerate the longitudinal (T_1) relaxation of water protons and therefore exhibit bright contrast where they localize. On the other hand, superparamagnetic iron oxide nanoparticles are used as T_2 contrast agents which accelerate the transverse (T_2) relaxation of (water) protons and exhibit dark contrast. The saturation magnetization of transition metals like cobalt is 1422 emu/cm^3,[25] which means that Co@C nanoparticles may have a larger effect on proton relaxation, leading to improved MR contrast. In this paper, the MR characterization of Co@C nanoparticles in solid phantoms is presented, demonstrating possible applications as MRI T_2 contrast agents.

Another promising application of the carbon coated magnetic nanoparticles is their use as hyperthermia agents. Magnetic hyperthermia is a method of selective heating of tissues by applying alternating (AC) magnetic fields. Most of the research in this area is concentrated on iron oxide nanoparticles.[26,27] Metallic materials could offer some advantages due to their superior magnetic properties. Recently, there were several works focused on carbon-coated metallic nanoparticles where the heating effect of these materials was shown.[21,28] However, the materials still need to be improved for safe usage in current anticancer therapies. Here, we present hyperthermia studies of Co@C nanoparticles which show high saturation magnetization and rather promising heating ability.

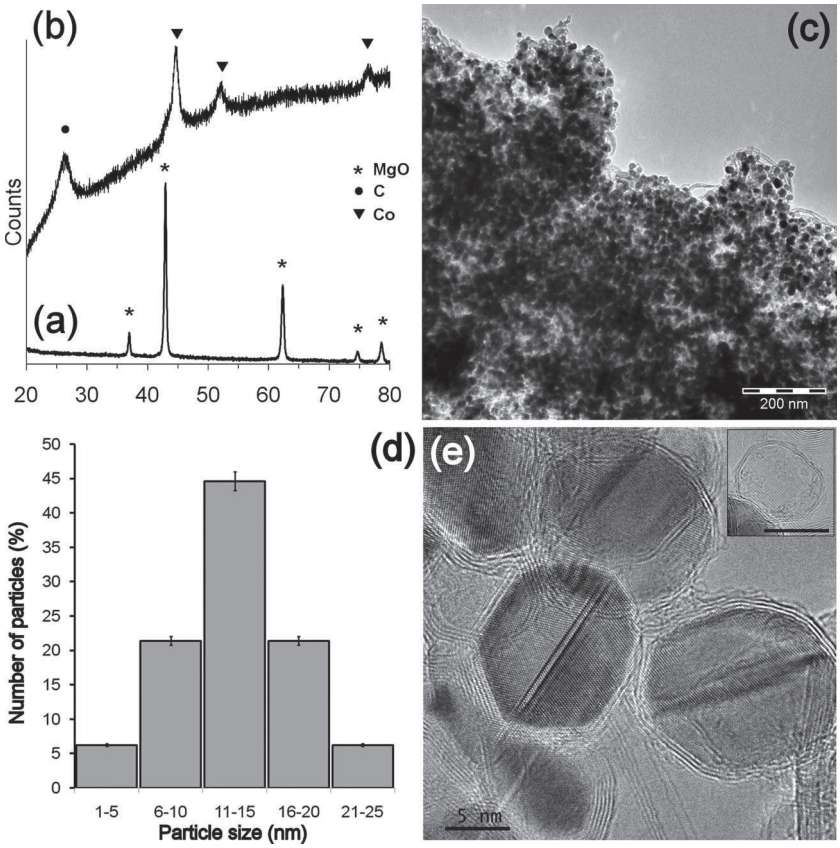

Figure 1. XRD patterns of a) C-Co-MgO nanocomposite powder and b) Co@C nanoparticles after HCl treatment; c) Low-magnification TEM image of Co@C nanoparticles after HCl treatment of the C-Co-MgO composite powder; d) particle size distribution of Co@C nanoparticles. e) HRTEM images of Co@C nanoparticles where the (fcc)-Co lattice is clearly visible, as well as the graphitic carbon shells. Inset (scale bar is 5 nm) shows empty carbon shells (metal removed);

2. Results and Discussion

Elemental analysis of the C-Co-MgO nanocomposite powder indicated a carbon content of 6.2 wt.%. After catalyst dissolution by HCl, the elemental analysis of the Co@C nanoparticles indicated that the sample contained 43 wt.% of C (almost 78 at.%), 56 wt.% of Co (21 at.%) and about 1 wt.% of oxygen.

X-ray diffraction (XRD) pattern (**Figure 1**a) of the C-Co-MgO nanocomposite powder exhibited peaks corresponding only to the MgO rock- salt lattice. The lack of peaks corresponding to Co oxides (CoO, Co_3O_4) in the diffractogram is an evidence that the Co ions are in solid solution in MgO. The XRD analysis of the black powder obtained after HCl treatment (Figure 1b) revealed only fcc-Co and C, evidencing the total dissolution of the MgO matrix. It is important to mention that no carbide (Co_3C) was found, in comparison to the synthesis of Fe@C nanoparticles[32] where Fe_3C is usually present in the samples. This is because Co_3C, if formed at high temperature during the synthesis, is not stable at room temperature, i.e., it decomposes to the elements Co and C when cooling from high temperature, which is probably the mechanism of formation of the Co@C nanoparticles.[15] Application of the Scherrer equation using the (111) peak gave a crystallite size of ca. 9 nm, which could be used as a mean diameter of Co nanoparticles (not including the carbon shells).

The TEM observation of Co@C nanoparticles (Figure 1c) showed that the sample was rather homogeneous, with only few carbon nanofibres. The sample contained nanoparticles

with a diameter ranging from 1 to 25 nm. Figure 1d shows that the sample contained about 46% of Co@C nanoparticles with an average diameter of 11–15 nm (diameter distribution was obtained by manual measurement of the diameter of 70 individual nanoparticles from TEM and HRTEM images). HRTEM observations (Figure 1e) indicated that the Co nanoparticles were coated, and thus protected, by two or three concentric carbon shells. It was observed that the Co nanoparticles size was not correlated with the number of surrounding carbon shells. However, if we consider that most Co@C nanoparticles were encapsulated within only 2 or 3 concentric shells, the size particle obtained from XRD data is in good agreement with HRTEM observations (ca. 10.4 nm for nanoparticles with 2 concentric shells, or ca. 11.1 nm in the case of nanoparticles with 3 concentric shells–using 0.345 nm as the distance between 2 consecutive carbon shells). We also observed the presence of empty carbon nanocapsules which gives some evidence that the non-protected Co metal was removed by the HCl treatment due to defective carbon structure.

The structural quality of the black C-Co solid was investigated by Raman spectroscopy. **Figure 2**a represents a typical Raman spectrum of Co@C nanoparticles, which exhibits only two peaks at 1324 cm^{-1} (D band) and 1588 cm^{-1} (G band). The G band corresponds to the carbon in sp^2 hybridization and it is associated with the E_{2g} mode (stretching vibration) in the basal-plane of graphite.[15] The D band at about 1344 cm^{-1} is due to the crystalline disorder and gives information about the level of sp^3 hybridization, corresponding to structural defects in the structure. We observed that the intensity ratio between the two bands is close to 1, which strongly suggests numerous structural defects (either carbon nanofibres, amorphous-like carbon deposit in the sample, or defects in the graphitic shells).

Table 1. Atomic concentration (%) of Co@C nanoparticles as calculated from XPS elemental spectra.

Sample	C1s		O1s		Co2p	
Co@C nanoparticles	%	E_b C1s [eV]	%	E_b O1s [eV]	%	E_bCo2p [eV]
	93.25	284.8	3.70	532.5	3.06	778.8

X-ray photoelectron spectroscopy (XPS) measurements were performed for the surface elemental analysis of Co@C nanoparticles after HCl treatment. XPS analysis of Co@C nanoparticles confirmed that there are no traces of MgO after HCl treatment (Figure 2b). The survey spectrum clearly shows the peaks corresponding to graphite, cobalt and oxygen. The atomic composition (at.%) of Co@C nanoparticles (**Table 1**) was calculated from elemental spectra. It shows that the percentage of oxygen is high compared to Co2p, which is probably due to oxygen chemisorbed onto the carbon outer layer. Taking into account the fact that the samples are likely to contain only C and Co elements, the wt.% can be converted to atomic% (at.%): the atomic concentration of C is 78%, and Co is 21%. However, from the elemental spectrum (Table 1) the atomic concentration of C1s is 93.25%, which is possibly due to the limitation of the penetration depth (~10 nm) of XPS analysis and/or to additional layers of carbon encapsulating the Co nanoparticles.

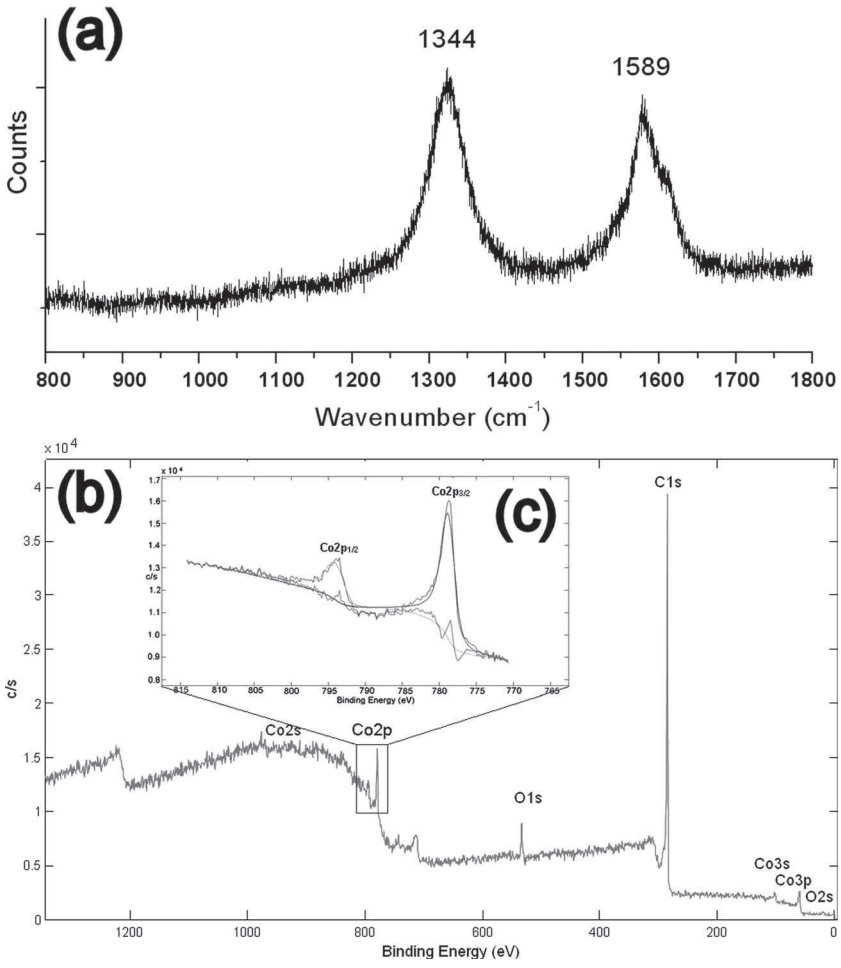

Figure 2. a) Raman spectra of Co@C nanoparticles exhibiting two bands (D at 1344 cm^{-1} and G at 1589 cm^{-1}); b) Normalized XPS survey spectrum; c) Co2p spectrum of Co@C nanoparticles after HCl treatment.

Figure 2c shows the XPS Co2p spectrum obtained from Co@C nanoparticles after HCl treatment. The main $Co2p_{3/2}$ peak on the XPS spectrum has a binding energy of 778.8 eV indicating the metallic state of cobalt nanoparticles,[33] which is consistent with the standard spectra of the element cobalt,[34] showing that the Co@C NPs are stable against further oxidation, thanks to tight encapsulation in the graphitic carbon shells.

Static magnetization measurements on the Co@C powder samples at room temperature (T = 300 K) revealed the ferromagnetic behavior of this material. The observed hysteresis loop is presented in **Figure 3**a. We measured a saturation magnetization M_S of 106 emu/$g_{Co@C}$ and a coercivity H_C of

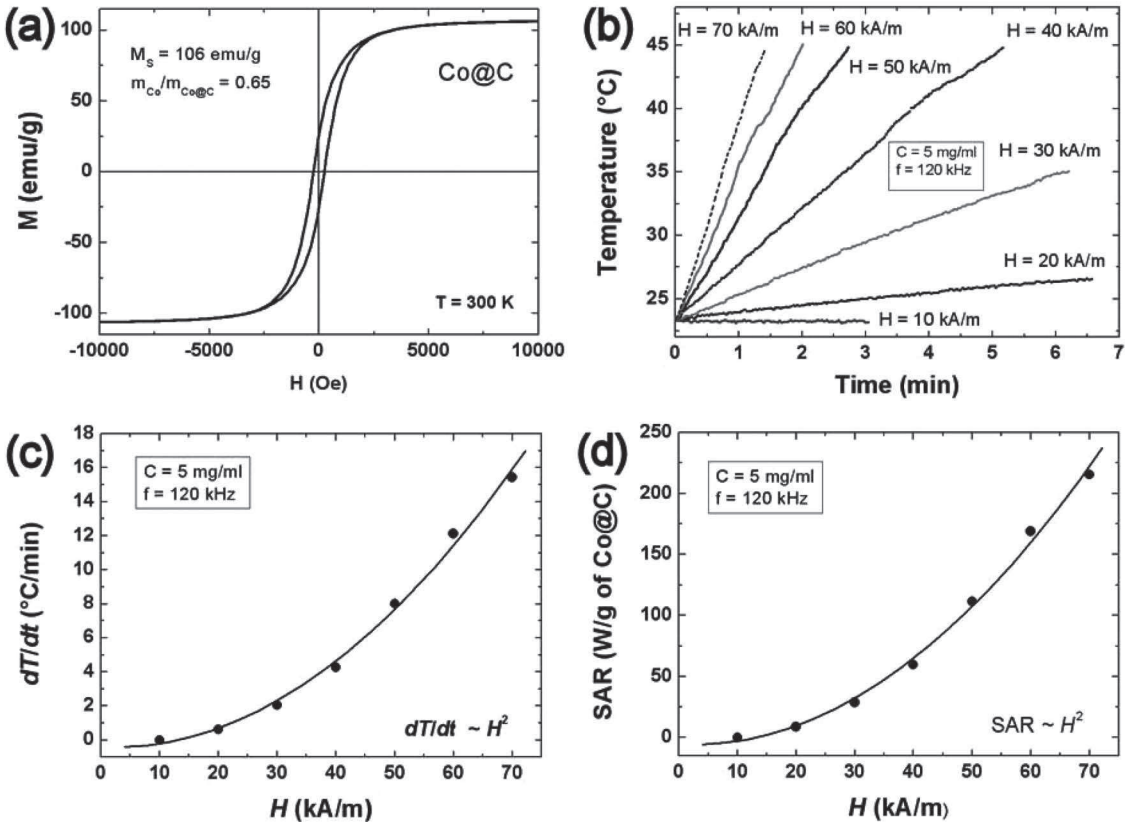

Figure 3. a) Magnetization of Co@C nanoparticles *vs.* applied magnetic field (hysteresis loop at room temperature (T = 300 K)). The data yield a saturation magnetization M_S of 106 emu/$g_{Co@C}$ and a coercitive field of 250 Oe; b) temperature increase with time of the Co@C dispersion at different AC magnetic fields strengths; c) Rate of temperature changes *vs.* AC magnetic field strength for the Co@C aqueous dispersion; d) specific absorption rate normalized by the weight of dry material *vs.* AC magnetic field strength.

250 Oe. The saturation magnetization agrees within the error bars with the Co amount deduced from the elemental analysis.

Calorimetry measurements on the Co@C aqueous dispersion showed a substantial temperature increase in applied AC magnetic fields starting from 20 kA/m (Figure 3b). The rate of temperature change is shown vs. AC magnetic field strength H in Figure 3c. The observed field dependence of the SAR ~ H^2 confirms the magnetic origin of the heating effect. At the highest applied magnetic field of 70 kA/m the temperature increase amounts to 15.4 °C/min. The calculated specific absorption rate (SAR) (mass normalized rate of energy absorption) related to the mass of the dry material is plotted vs. H in Figure 3d. Note, that the observed values of the SAR (e.g., 28.7 W/$g_{Co@C}$ at 30 kA/m and 215.4 W/$g_{Co@C}$ at 70 kA/m) are slightly lower than required in actual hyperthermia therapies (according to the magnetic field/frequency limitation $fH < 4.9 \cdot 10^8$ $Am^{-1}s^{-1}$).[35] However, the observed strong heating effects provide a very promising starting point for future clinical application.

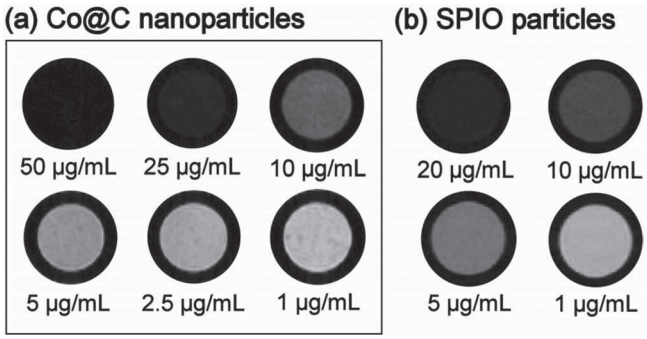

Figure 4. T_2-weighted MR contrast images: a) Co@C nanoparticles in solid phantoms, b) super-paramagnetic iron oxide (SPIO) particles in solid phantoms. T_2-weighted multi-slice multi echo (MSME) sequence is used with a pulse repetition time (TR) of 2000 ms, flip angle of 180°, echo time (TE) of 30 ms and slice thickness of 2 mm.

For MR Imaging the Co@C nanoparticles were dispersed in glass capillary tubes (outer diameter ~1000 µm) containing 1.5% (w/v) of Agar at different concentrations from 1 to 50 µg/mL. **Figure 4**a shows the T_2-weighted image of Co@C nanoparticles with CMC in solid phantoms. Figure 4b shows the T_2-weighted image of commercially available superparamagnetic iron oxide (SPIO) nanoparticles (Endorem™ Guerbert, earlier trade name AMI-25, Laboratoire Guerbert, France) in solid phantoms. Multislice multi echo (MSME) sequence was used for T_2-weighted Images with Repetition Time (T_R) of 2000 and Echo Time (T_E) of 30 ms. The minimum concentration of Co@C nanoparticles required to see the negative contrast in T_2-weighted images is 5 µg/mL. The T_2-weighted image

showed negative contrast by increasing the concentration of Co@C nanoparticles in microgram level, which is similar to commercially available T_2 contrast agents (SPIO nanoparticles). Hence, together with therapeutic applications, Co@C nanoparticles also have potential diagnostic applications as MRI contrast agents. The cytotoxicity of Co@C nanoparticles was evaluated by measurement of metabolic activity of cells after exposure to different concentrations of nanoparticles (WST-1 test) and by the clonogenic survival assay of cells seeded in the presence of the nanoparticles. The cell line used for these studies was DU-145 (brain metastasis of prostate cancer). The biocompatibility tests of Co@C nanoparticles showed that cell viability was statistically affected only by high concentrations (50 μg/mL). In comparison, commercial Fe@C nanoparticles (Nanomaterial Store: FeNP (SN1501)) statistically decreased cell viability from only 10 μg/mL in the same experimental conditions (these data will be published in a more specialised journal).

3. Conclusions

In this work we describe an easy and cheap method for synthesis of carbon-encapsulated cobalt nanoparticles with an average diameter of 1–25 nm. Fcc-Co nanoparticles are encapsulated within two or three carbon shells, which efficiently protect the metal from air oxidation. These carbon shells could also be used for attaching different functional groups in order to make the particles easy to disperse in different solutions typically used for biomedical applications. We tested the heating ability of the Co@C nanoparticles in AC magnetic fields and observed a substantial temperature increase in the liquid dispersion. These results give some strong evidence of the feasibility of the use of such nanoparticles for contactless magnetic heating. We have also demonstrated the potential biomedical application of Co@C nanoparticles as T_2 MRI contrast agents (CA). Even if they are not used for this purpose, they could at least be monitored by MRI after injection in the body.

4. Experimental Section

The solid solution of $Mg_{0.92}Co_{0.08}O$ was prepared by ureic combustion method starting from an aqueous solution of $Mg(NO_3)_2{\cdot}6H_2O$ and $Co(NO_3)_2{\cdot}6H_2O$ (purity > 99%, *Prolabo*). The metal nitrates and urea were mixed in stoichiometric proportion. The stoichiometric composition of the redox mixture was calculated using the total oxidizing and reducing valency of the metal nitrates (oxidizer) and urea (fuel), so that the equivalence ratio was equal to unity.[29,30] After dissolution of the precursors in deionised water, the solution was placed in an open furnace preheated at 550 °C (in air). The solution immediately started to boil and underwent dehydration before ignition (presence of a flame). The total combustion process was over in less than 5 min and the obtained solid was then gently ground using a mortar and pestle. In order to eliminate the carbon contamination (residues of the decomposition of excess urea), the sample was calcined at 550 °C for 1 h (in air).

7 g of solid solution were placed in a furnace and heated up to 900 °C (5 °C/min) in a flow of H_2 (5 L/h). After reaching this temperature, the H_2 was replaced by CH_4 (20 L/h) for 5 min (dwell). The sample was then cooled down in N_2 at 5 °C/min to room temperature. The C-Co-MgO product was then treated with concentrated HCl [16] to dissolve the unreacted catalyst as well as non-protected metal nanoparticles. Typically, 70 mL of concentrated HCl (15 M) were added to 7 g of the C-Co-MgO nanocomposite powder, followed by bath ultrasonication for 15 min after what the suspension rested overnight at room temperature. The blue Co(II) suspension and the black solid were separated by filtration using a Cellulose Nitrate filtration membrane (pore size 0.45 μm), followed by washing with deionised water until neutrality. The final product (Co@C nanoparticles) was dried at 80 °C overnight.

The carbon content was determined by flash combustion with an accuracy of 2 wt.%. Flash combustion is based on the complete and instantaneous oxidation of the sample; carbon is oxidized into CO_2 which is detected by a thermal conductivity detector, giving an output signal proportional to the concentration in the sample. Elemental analysis was obtained by Atomic Absorption Spectroscopy with an accuracy of 1 wt.%.

X-Ray diffraction (XRD) patterns were obtained using Cu-Kα radiation (λ = 0.15418 nm, Bruker Endeavor D4). The product was observed by transmission electron microscopy (TEM) using both at high-resolution JEOL 2100F (HRTEM) operated at 200 kV and at lower magnification with a JEOL 1011 (TEM) microscope operated at 100 kV. The Raman characterization of samples was done at the Common Service of spectroscopy of the University Paul Sabatier with a LabRAM HR 800 spectrometer (Jobin Yvon). The wavelength of the laser was 633 nm (red laser). Magnetic properties have been measured using an AGM (Alternating Gradient Magnetometer) MicroMag Model 2900 from Princeton Measurement Corporation. The samples were investigated as dry powders (0.5 mg of sample). The field dependence of the static (DC) magnetization M(H) was measured at room temperature in magnetic fields up to 1 T. The heating effect of Co@C nanoparticles in alternating magnetic fields was studied using a home-made experimental setup which consists of a high-frequency generator with an impedance matching network and a water-cooled magnetic coil system. The coil contains five turns; the height of the coil is 40 nm and the diameter of the inside core is 30 mm. For such a coil geometry the setup provides alternating magnetic fields with a frequency f = 139 kHz and a magnetic field strength *H* of 0–120 kA/m. Thermal insulation of the samples during the measurements was provided by placing the material in an evacuated glass Dewar vessel centered within the coil. The temperature was determined by means of a fiber optical temperature controller (Luxtron One), which is suitable for measurements in high-frequency magnetic fields.

X-ray photoelectron spectrometer (XPS, Quantera SXM scanning electron microprobe, Physical Electronics) with monochromated Al Kα X-ray at 1486.6 eV, a power of X-ray beam of 25.3 W, pass energy of 224 eV, scanning area of 600 μm × 300 μm, was used to analyze the elemental composition of Co@C nanoparticles and also to check the oxidation state of cobalt after catalyst elimination (acid treatment). MR imaging experiments on Co@C nanoparticles in solid phantoms were performed on a 600 MHz Avance II NMR spectrometer from Bruker (Karlsruhe, Germany) equipped with a vertical narrow bore magnet (14.1 T), a Great B_o compensation unit (BGU-II) and 3 Great 1/60 amplifier units (X, Y and Z), together with ParaVision version 4 software. A micro 5 imaging probe equipped with a 10 mm diameter saddle coil insert from Bruker (Karlsruhe, Germany) was used, with maximum gradient strength of 4.8 G/cm/A and the inside temperature of the sample was kept at ~25 °C by a BCU20 water cooling unit. For uniform dispersions, Co@C nanoparticles were suspended in distilled water containing 1% of carboxyl-methyl-cellulose (CMC) sodium salt (Sigma-Aldrich Corp St. Louis, MO USA). The dispersions were sonicated with an ultrasonic tip (Biologics, Inc. ultrasonic homogenizer 150VT with tapered titanium micro tip with a diameter of 1.6 mm) in plastic test tubes at an average power of 20 W for 2–3 min (with 30 s ON/OFF cycle in order not to overheat the sample) while cooling in an ice bath. Tissue mimicking solid phantoms were prepared by using Agar (Sigma-Aldrich Corp St. Louis, MO USA) as a base material.[31] For MR imaging, samples (Co@C nanoparticles in solid phantoms) were prepared in glass capillary tubes (outer diameter ~1000 μm) purchased from Hirschmann Laborgeräte GmbH & Co.KG (Eberstadt, Germany), NMR tubes (10 mm diameter) were purchased from Wilmad Labglass (New Jersey, U.S.A).

Acknowledgements

We thank the European FP6 RTN CARBIO (contract number: MRTN-CT-2006-035616) (www.carbio.eu) for the financial support.

[1] G. Cui, Y.-S. Hu, L. Zhi, D. Wu, I. Lieberwirth, J. Maier, K. Müller, *Small* **2007**, *12*, 2066.
[2] C. Corot, P. Robert, J. M. Idee, M. Port, *Adv. Drug Deliv. Rev.* **2006**, *58*, 1471.
[3] D. K. Kim, Y. Zhang, W. Voit, K. V. Rao, M. Muhammed, *J. Magn. Magn. Mater.* **2001**, *30*, 222.
[4] E. Sutter, P. Sutter, *Adv. Mater.* **2006**, *18*, 2583.
[5] E. Sutter, P. Sutter, R. Calarco, T. Stoica, R. Meijers, *Appl. Phys. Lett.* **2007**, *90*, 093118-1.
[6] J. Geng, D. A. Jefferson, B. F. G. Johnson, *Chem. Commun.* **2004**, 2442.
[7] Q. A. Pankhurst, J. Connolly, S. K. Jones, J. Dobson, *J. Phys. D: Appl. Phys.* **2003**, *36*, R167.
[8] C. Sun, J. S. H. Lee, M. Zhang, *Adv. Drug Deliv. Rev.* **2008**, *60*, 1252.
[9] M. Bystrzejewski, A. Huczko, H. Lange, *Sens. Actuat., B* **2005**, *109*, 81.
[10] Y. Wang, Z. Wang, *Chem. Mater.* **2001**, *13*, 1008.
[11] R. Ruoff, D. Lorents, B. Chan, R. Malhotra, S. Subramoney, *Science* **1993**, *259*, 346.
[12] Y. Saito, T. Yoshikawa, M. Okuda, N. Fujimoto, S. Yamamuro, K. Wakoh, K. Sumiyama, K. Suzuki, A. Kasuya, *J. Appl. Phys.* **1994**, *75*, 134.
[13] Y. Saito, *Carbon* **1995**, *33*, 979.
[14] Z. Liu, Z. Yuan, W. Zhou, Z. Xu, L. Peng, *Chem. Vap. Deposition* **2001**, *7*, 248.
[15] E. Flahaut, F. Agnoli, J. Sloan, C. O'Connor, M. L. H. Green, *Chem. Mater.* **2002**, *14*, 2553.
[16] E. Flahaut, A. Peigney, Ch. Laurent, A. Rousset, *J. Mater. Chem.* **2000**, *10*, 249.
[17] W. Seo, Jin. Lee, X. Sun, Y. Suzuki, D. Mann, Z. Liu, M. Terashima, P. Yang, M. McConnell, D. Nishimura, H. Dal, *Nat. Mater.* **2006**, *5*, 971.
[18] C. He, N. Zhao, C. Shi, X. Du, J. Li, *J. Alloys Comp.* **2009**, *472*, 230.
[19] N. Chopra, L. Bachas, M. Knecht, *Chem. Mater.* **2009**, *21*, 1176.
[20] X. Wang, B. Xu, X. Liu, J. Guo, H. Ichinose, *Diam. Relat. Mater.* **2006**, *15*, 147.
[21] A. El-Gendy, E. Ibrahim, V. Khavrus, Y. Krupskaya, S. Hampel, A. Leonhardt, B. Buchner, R. Klingeler, *Carbon* **2009**, *47*, 2821.
[22] S. Pol, V. Pol, A. Frydman, G. Churilov, A. Gedanken, *J. Phys. Chem. B* **2005**, *109*, 9495.
[23] P. Caravan, *Chem. Soc. Rev.* **2006**, *35*, 512.
[24] W. M. B. Jeff, L. K. Dara, *NMR Biomed.* **2004**, *17*, 484.
[25] L. M. Parkes, R. Hodgson, L. T. Lu, L. D. Tung, I. Robinson, N. T. K. Thanh, *Contrast Media Mol. Imaging* **2008**, *3*, 150.
[26] A. Jordan, R. Scholz, K. Maier-Hauff, M. Johannsen, P. Wust, J. Nadobny, H. Schirra, H. Schmidt, S. Deger, S. Loening, W. Lanksch, R. Felix, *J. Magn. Magn. Mater.* **2001**, *225*, 118.
[27] R. Hergt, R. Hiergeist, M. Zeisberger, G. Glockl, W. Weitschies, L. P. Ramirez, I. Hilger, W. A. Kaiser, *J. Magn. Magn. Mater.* **2004**, *280*, 358.
[28] Y. Krupskaya, C. Mahn, A. Parameswaran, A. Taylor, K. Kraemer, S. Hampel, A. Leonhardt, M. Ritschel, B. Buechner, R. Klingeler, *J. Magn. Magn. Mater.* **2009**, *321*, 4067.
[29] K. C. Patil, *Bull. Mater. Sci.* **1993**, *16*, 533.
[30] A. Cordier, A. Peigney, E. De Grave, E. Flahaut, Ch. Laurent, *J. Eur. Ceram. Soc.* **2006**, *26*, 3099.
[31] R. Cubeddu, A. Pifferi, P. Taroni, A. Torricelli, G. Valentini, *Phys. Med. Biol.* **1997**, *42*, 1971.
[32] J. Geng, D. A. Johnson, B. F. G. Johnson, *Chem. Commun.* **2004**, *21*, 2442.
[33] J. F. Moulder, W. F. Stickle, P. E. Sobol, K. D. Bomben, *Handbook of X-ray Photoelectron Spectroscopy*, Perkin-Elmer Corporation, Eden Prairie, USA **1992.**
[34] N. Ikeo, Y. Iijima, N. Niimura, M. Sigematsu, T. Tazawa, S. Matsumoto, K. Kojima, Y. Nagasawa, *Handbook of X-ray Photoelectron Spectroscopy*, *JEOL ltd*. Japan **1991**
[35] R. Hergt, S. Dutz, *J. Magn. Magn. Mater.* **2007**, *311*, 187.